Ionics (2021) 27:213–224
https://doi.org/10.1007/s11581-020-03777-1

ORIGINAL PAPER

Analytical modeling of solution-phase diffusion in porous composite electrodes under time-dependent flux boundary conditions using Green's function method

Mohammad Parhizi[1] · Ankur Jain[1]

Received: 4 May 2020 / Revised: 12 August 2020 / Accepted: 7 September 2020 / Published online: 7 October 2020

Abstract

Mathematical modeling of species transport in a Li-ion cell is important for understanding and optimizing the performance of Li-ion cells in a wide variety of energy conversion and storage processes. Specifically, solid- and liquid-phase diffusion in the electrodes is an important process that governs cell performance. Most analytical and numerical models developed in the past have focused on a constant current boundary condition. However, time-dependent boundary conditions may be important in many applications, where the applied charging or discharging current changes with time. This paper presents an analytical solution for the solution-phase diffusion limitation problem for a composite electrode operating under time-dependent flux boundary condition and arbitrary initial conditions using the Green's function approach. Results based on the analytical solution show good agreement with past work for constant current boundary conditions, as well as numerical simulation results. The results are used to predict the concentration distribution for linear, periodic, and step-function variations in current density as a function of time. Results from the step-function boundary condition address practical applications where sudden changes in the magnitude and direction of the imposed current may occur. Results derived for periodic functions are also of practical significance since other current profiles can be represented by series comprising periodic functions. This work expands the theoretical understanding of diffusion in Li-ion cells, and provides the basis for understanding and optimizing important charge/discharge processes in Li-ion cells.

Keywords Li-ion cells · Solution-phase diffusion · Porous electrode · Analytical modeling · Green's function

Nomenclature

a	Specific interfacial area (m^{-1})
c	Non-dimensional concentration, $c = C/C_0$
C_0	Reference concentration (mol m^{-3})
C	Concentration (mol m^{-3})
D	Diffusion coefficient of electrolyte in the solution (m^2s^{-1})
$f(x)$	Non-dimensional initial concentration, $f(x) = F(x)/C_0$
$F(x)$	Initial concentration (mol m^{-3})
F	Faraday's constant (C mol^{-1})
g	Non-dimensional generation or consumption
G	Green's function
I	Current density (A/m^2)
j_n	Pore wall flux, $j_n = -I/aFL_c$ (mol m^{-2} s^{-1})
J	Non-dimensional pore wall flux, $J = -I(1-t^+)L_s^2/FDL_cC_0$
k	Non-dimensional constant
L_s	Length of the separator (m)
L_c	Length of the porous electrode (m)
r	Ratio of electrode length to separator length, $r = L_c/L_s$
t	Non-dimensional time, $t = D\tau/L_s^2$
t^+	Transference number
x	Non-dimensional lengthscale, $x = X/L_s$
X	Lengthscale (m)
α	Non-dimensional constant
ε	Porosity
ω	Non-dimensional frequency
τ	Time (s)
λ	Eigenvalues

Subscripts

c	Cathode

✉ Ankur Jain
jaina@uta.edu

[1] Mechanical and Aerospace Engineering Department, University of Texas at Arlington, 500 W First St, Rm 211, Arlington, TX 76019, USA

h Homogeneous problem
s Separator

Introduction

Li-ion batteries are among the most popular rechargeable batteries for a wide variety of applications due to their promising electrochemical characteristics [1–3]. Favorable characteristics of Li-cells include high energy density, high power density, low self-discharge rate, stability, and long cycle life [4–6]. The operation of Li-ion cells involves coupled thermal and electrochemical processes such as kinetic reactions, mass, charge, and thermal transport phenomena [7, 8]. Mathematical modeling of Li-ion cells is, therefore, necessary to fully understand the underlying processes towards design and optimization of electrochemical energy conversion and storage systems [9, 10].

Extensive research has been reported towards development of theoretical models to predict electrochemical and thermal transport in Li-ion cells subject to different operating conditions [11, 12]. These electrochemical models solve the underlying charge, mass, and thermal transport equations, as well as reaction kinetics [11–14]. Two most extensively used electrochemical models are the pseudo-2D model (P2D) and single particle model (SPM) [11]. P2D model was constructed based on the porous electrode theory introduced by Newman [15] and the concentrated solution theory [16]. It solves the species and charge transport in both solution and solid phases [11, 17]. P2D model is generally coupled and non-linear, resulting in a large number of equations and significant computational time. Thus, single particle model (SPM) was developed to reduce the complexity associated with P2D model. In SPM, concentration gradients in the solution phase are neglected, leading to dominance of solid-phase diffusion in the porous electrode, which can be represented by a single, one-dimensional particle [8, 18, 19]. At low discharge rates and for thin electrodes, this may be a reasonable assumption [20, 21]. However, at larger discharge rates or for thick electrodes, for example energy cells, when concentration gradient in the solution phase cannot be neglected, the governing equations become coupled and simplification is needed in order to derive an analytical solution. Towards this, Doyle et al. [22] assumed a specific form for the reaction rate distribution in the porous electrode, leading to uncoupling of the governing equations. Based on this approach, analytical solutions have been derived using the separation of variables (SOV) method for three limiting cases—solid phase, solution phase, and ohmically dominated cell [22]. The governing equations in the solid phase were defined based on Fick's law, and the material balance in the solution phase was defined using the concentrated solution theory [22].

A variety of approximate analytical methods have been developed, including the parabolic profile (PP) method [23, 24], state variable model (SVM) [25, 26], extended single particle model (ESPM) [27, 28], proper orthogonal decomposition (POD) [29], and electrode averaged model (EAM) [30]. Due to the coupled and non-linear nature of the underlying equations, exact solutions are available only for a limited number of problems. For example, an extended SOV technique has been used to predict concentration profile in both solid- and liquid-phase diffusion problems in composite electrodes under constant galvanostatic discharge boundary condition and zero initial concentration [31]. An exact solution has been presented for solid-phase diffusion in a spherical particle under time-dependent flux boundary condition using finite integral transform technique [32]. Material balance equations in thin film, cylindrical, and spherical electrodes under galvanostatic boundary condition have been solved using integral transform method [33]. Exact solution for both solid- and solution-phase diffusion with non-zero initial condition has been developed using Laplace transformation technique [34]. Green's function approach has been used to solve the solution-phase diffusion in composite electrode for a constant boundary condition [35].

The diffusion problem in Li-ion cells is inherently multilayer in nature, involving diffusion through the electrodes as well as the separator. A number of papers have presented analysis of multilayer diffusion problems through a variety of theoretical methods, such as eigenvalue methods [36, 37], Laplace transforms [38], and variable substitution followed by use of Vodicka-type orthogonality [39]. Time-dependent boundary conditions have been accounted for using Duhamel theorem [40] as well as Laplace transforms [41]. For eigenvalue-driven approaches, computation of eigenvalues is often challenging for a multilayer geometry [36].

While these methods have been discussed for a variety of applications such as heterogeneous porous media [38], geology [42, 43], and semiconductor devices [44], there is a relative lack of similar work on multilayer diffusion in Li-ion cells. Specifically, most of the past work in this field assumes constant boundary conditions and constant generation/consumption rate. While time-dependent boundary conditions have been modeled for general problems [41, 45], there is a lack of such work in the specific context of Li-ion cells. Time-dependent boundary conditions may be important in practical applications involving Li-ion cells, where the applied charging or discharging current changes with time. This could occur, for example, in an electric vehicle battery pack where the discharge rate changes with time due to changes in the driving load. In some cases, the cell may even switch between charge and discharge. Only a few analytical and approximate solutions have been presented to address such problems with time-dependent boundary conditions. For example, finite integral transform method has been used to develop an exact solution

for solid-phase diffusion in a single spherical porous electrode operation under arbitrary initial and boundary conditions [32]. Green's function approach has been used to solve the solid-phase diffusion in single layer and composite electrodes [46]. Approximate solutions have been presented for solid-phase diffusion limitation single-layer electrode under time-dependent boundary conditions [28].

In light of the relative lack of analytical solutions for problems with time-dependent boundary conditions, time-dependent generation/consumption rate, and an arbitrary space-dependent initial concentration, mathematical modeling of such problems may be of much interest. A feasible approach for providing solutions to such problems is the use of Green's function technique. Green's functions have been used commonly for heat transfer problems with complicated geometry and boundary/initial conditions [47], including the use of techniques such as method of fundamental solutions [42] and singular boundary method [43]. Green's function has been used for solving multilayer problems in biotransport [48] and multilayer materials [49]. However, only limited use of Green's function approach exists for addressing species transport problems in electrochemical systems [35, 46].

This paper presents an analytical solution for Li-ion diffusion in a composite porous electrode operating under time-dependent flux boundary condition and arbitrary initial conditions using Green's function approach. Solid-phase diffusion limitation is neglected and the solution-phase diffusion limitation is dominant, which is one of the limiting cases of Li-ion cell operation [22]. While the reaction term in the species conservation equation is, in general, a function of both and time, under solution-phase diffusion limitation, this term has been treated to be a constant [22]. The present work generalizes this by considering a time-dependent function, which may occur when the external current changes with time, for example during cyclic charge/discharge of the battery pack of an electric vehicle. Also, note that the governing equations in this study are presented for a single insertion electrode but the results can be easily generalized to two insertion electrodes. The analytical model presented in this paper provides a useful mathematical tool to understand transport phenomena in a porous Li-ion cell, which may improve the analysis and design of electrochemical energy storage and conversion devices.

Mathematical Modeling

Green's Function Approach for Composite Electrodes

Heat and mass transport are often governed by similar diffusion equations. If the non-homogeneities in these equations are arbitrary functions of time, the commonly used SOV method may not be readily applicable. On the other hand, Green's function approach continues to be a powerful mathematical tool for solving a wide range of linear partial differential equations with arbitrary time-dependent non-homogeneities in the governing equation and boundary conditions [47, 50]. Green's function method can be used to address species diffusion problems in single- or multi-layer bodies.

Consider diffusion in a M-layer composite body shown in Fig. 1. In general, each layer may have different properties and species consumption/generation due to reaction. In addition, two time-dependent flux boundary conditions are considered at the two ends. The governing conservation equation can be written in non-dimensional form as:

$$\alpha_i \frac{1}{x^p}\frac{\partial}{\partial x}\left(x^p \frac{\partial c_i}{\partial x}\right) + \frac{\alpha_i}{k_i} g_i(x,t) = \frac{\partial c_i}{\partial t} \quad x_i < x < x_{i+1} \tag{1}$$

subject to the following general boundary and initial conditions:

$$-k_1 \left(\frac{\partial c_1}{\partial x}\right)_{x=x_1} = q_1(\tau) \quad at\ x = x_1 \tag{2}$$

$$c_i\big|_{x=x_{i+1}} = c_{i+1}\big|_{x=x_{i+1}} at\ interfaces\ i = 1, 2, \ldots, M-1 \tag{3}$$

$$k_i \left(\frac{\partial c_i}{\partial x}\right)_{x=x_{i+1}} = k_{i+1}\left(\frac{\partial c_{i+1}}{\partial x}\right)_{x=x_{i+1}} \quad at\ interfaces\ i = 1, 2, \ldots, M-1 \tag{4}$$

$$-k_M \left(\frac{\partial c_M}{\partial x}\right)_{x=x_{M+1}} = q_M(\tau) \quad at\ x = x_{M+1} \tag{5}$$

$$c_i = f_i(x) \quad at\ t = 0 \tag{6}$$

where x'^p is the Sturm–Liouville weight function, and $p = 0$, 1, and 2 for slabs, cylinders, and spheres, respectively. α and k are constants and can be determined based on a specific problem. Here, Eqs. (3) and (4) represent continuity of species and flux balance at the interfaces, whereas Eqs. (2) and (5) represent a balance between diffusion and mass flux at the two ends. f is the initial condition, g is the generation or consumption term, and $q(\tau)$ is the non-homogeneous boundary condition.

The solution to this multi-layer diffusion problem using Green's function approach is given by [47]:

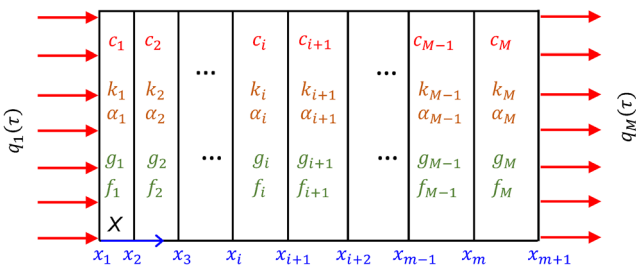

Fig. 1 Schematic of a M-layer composite electrode

$$c_i(x,t) = \sum_{j=1}^{M} \left\{ \int_{x'=x_j}^{x_{j+1}} G_{ij}\left(x,t|x',t'\right)_{t'=0} f_j\left(x'\right) x'^{p} dx' + \int_{t=0}^{t} \int_{x'=x_j}^{x_{j+1}} G_{ij}\left(x,t|x',t'\right) \frac{\alpha_j}{k_j} g_j\left(x',t'\right) x'^{p} dx' dt' \right\} + \sum_{m=1,M} \frac{\alpha_m}{k_m} \int_{t'=0}^{t} \left[x'^{p} G_{im}\left(x,t|x',t'\right) \right]_{x=x_{b,m}} q_m\left(t'\right) dt' \quad (7)$$

where the summation in the third term is taken over all layers with an external boundary. $x_{b,m}$ refers to the location of the external boundary for the m^{th} layer (referring to Fig. 1, $x_{b,1} = x_1$, and $x_{b,M} = x_{M+1}$).

The first term in Eq. (7) accounts for the initial condition, while the second and third terms represent contributions of non-homogeneities in the governing equation and boundary conditions, respectively. The solution represented by Eq. (7) is particularly powerful in its ability to account for the effect of arbitrary space-dependent initial condition, time- and space-dependent generation/consumption, and time-dependent boundary conditions.

A key step in deriving the Green's function-based solution for the specific problem under consideration is to determine the Green's function $G(X, \tau|X', \tau')$ that appears in Eq. (7). To do so, the corresponding homogeneous version of the problem must be solved first. For a homogeneous problem, the only non-zero term in Eq. (7) is the first term which represents the contribution of the initial concentration. Thus, a comparison between the first term in Eq. (7) and the solution to the homogeneous problem results in the evaluation of the Green's function at $t' = 0$, $G\left(x,t|x',t'\right)_{t'=0}$. In order to determine the complete Green's function at any time, t, i.e. $G(x, t|x', t')$, t must be replaced with $(t - t')$ in $G\left(x,t|x',t'\right)_{t'=0}$.

The next sections present the problem statement and derivation of the solution for liquid-phase diffusion in a porous Li-ion cell sandwich under an arbitrary time-dependent flux using Green's function method.

Governing Equations and Boundary Conditions

Figure 2 shows a schematic of a Li-ion cell sandwich comprising a porous electrode, separator, and Li-ion foil electrode. The separator and porous electrode, referred to with subscripts 1 and 2, respectively, are initially at a non-uniform concentration of $F_1(x)$ and $F_2(x)$. The cell sandwich operates under a time-dependent discharge boundary condition, $q(\tau)$ at $X = 0$. Doyle and Newman presented governing equations for composite Li-ion cell sandwich under a uniform current distribution [22]. Note that the reaction rate distribution in the electrode is, in general, a function of both location and time, $J(x,t)$. However, under the solution-phase diffusion limitation, the spatial distribution of the reaction term can be neglected [22]. When the external current on the cell is a function of time, as may be the case during cyclic charge and discharge of

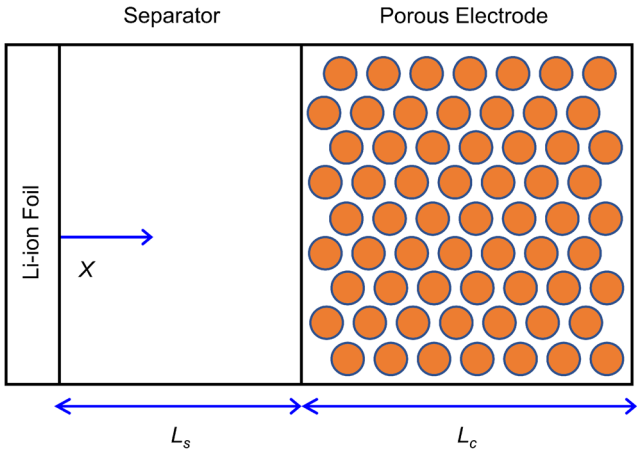

Fig. 2 Schematic of the composite porous electrode consisting of Li-ion foil, separator, and positive porous electrode

a Li-ion cell in an electric vehicle, the reaction term is, in general, a function of time. Neglecting solid-phase diffusion limitation, conservation equations for the separator and porous electrodes for this case can be written as:

$$D\frac{\partial^2 C_1}{\partial X^2} = \frac{\partial C_1}{\partial \tau} \quad 0 < X < L_s \quad (8)$$

$$D\varepsilon^{3/2}\frac{\partial^2 C_2}{\partial X^2} + aj_n(\tau)(1-t^+) = \varepsilon\frac{\partial C_2}{\partial \tau} \quad L_s < X < L_s + L_c \quad (9)$$

Subject to the following boundary conditions:

$$D\left(\frac{\partial C_1}{\partial X}\right)_{X=0} = -\frac{I(\tau)(1-t^+)}{F} \; at\; X = 0 \quad (10)$$

$$C_1 = C_2 \quad at\; X = L_s \quad (11)$$

$$\left(\frac{\partial C_1}{\partial X}\right)_{X=L_s} = \varepsilon^{3/2}\left(\frac{\partial C_2}{\partial X}\right)_{X=L_s} \quad at\; X = L_s \quad (12)$$

$$\left(\frac{\partial C_2}{\partial X}\right)_{X=L_s+L_c} = 0\; at\; X = L_s + L_c \quad (13)$$

The initial conditions are:

$$C_1 = F_1(X) \quad at\; \tau = 0 \quad (14)$$

$$C_2 = F_2(X) \quad at\; \tau = 0 \quad (15)$$

where D, ε, and a refer to diffusion coefficient of the electrolyte, porosity of the electrode, and specific interfacial area, respectively. I, j_n, t^+, and F refer to current density, pore wall flux, transference number, and Faraday constant, respectively. L_s and L_C are the separator and porous electrode lengths, respectively. Note that Eqs. (8) and (9) describe diffusion in the separator and material balance in the solution phase of the porous electrode, respectively. Equation (10) describes the

time-dependent flux boundary condition. Equations (11) and (12) ensure the continuity of concentration and flux at the separator-electrode interface. Equation (13) ensures that no ions diffuse through the back of the electrode, and finally, Eqs. (14) and (15) represent the initial condition.

The current distribution is assumed to be time-dependent and uniform throughout the electrode. While in general, the reaction rate distribution might be quite complicated and non-uniform [22], it has been shown that if the kinetic resistance dominates ohmic resistance, the reaction rate distribution can be considered as its average value throughout the electrode [15].

Note that, in case of uniform initial concentration, the two non-homogeneities driving this problem during discharge are concentration flux into the separator (Eq. (10)) and species consumption due to lithium intercalation in the cathode (Eq. (9)). The interplay between the two processes over time determines how the concentration field changes with time.

For a uniform current distribution, j_n can be written as its average value everywhere in the porous electrode [22] as follows:

$$j_n(\tau) = \frac{-I(\tau)}{aFL_c} \tag{16}$$

Using the non-dimensionalization scheme presented in the Nomenclature section, and after some mathematical simplification, the non-dimensional form of the governing equations for the separator and electrode can be written as:

$$\frac{\partial^2 c_1}{\partial x^2} = \frac{\partial c_1}{\partial t} \quad 0 < x < 1 \tag{17}$$

$$\varepsilon^{1/2}\frac{\partial^2 c_2}{\partial x^2} + \frac{\varepsilon^{1/2}}{\varepsilon^{3/2}}J(t) = \frac{\partial c_2}{\partial t} \quad 1 < x < 1 + r \tag{18}$$

where $J(t) = \frac{-I(t)(1-t^+)L_s^2}{FDL_cC_0}$. The associated boundary conditions are:

$$\left(\frac{\partial c_1}{\partial x}\right)_{x=0} = J(t)r \quad at\ x = 0 \tag{19}$$

$$c_1 = c_2 \quad at\ x = 1 \tag{20}$$

$$\left(\frac{\partial c_1}{\partial x}\right)_{x=1} = \varepsilon^{3/2}\left(\frac{\partial c_2}{\partial x}\right)_{x=1} \quad at\ x = 1 \tag{21}$$

$$\left(\frac{\partial c_2}{\partial x}\right)_{x=1+r} = 0 \quad at\ x = 1 + r \tag{22}$$

The initial conditions for the separator and electrode are:

$$c_1 = f_1(x) \quad at\ t = 0 \tag{23}$$

$$c_2 = f_2(x) \quad at\ t = 0 \tag{24}$$

Comparison between Eqs. (17)–(24) specific to this problem and the general problem statement for Green's function solution given by Eqs. (1)–(6) indicate that, in this case, $M = 2$, $\alpha_1 = 1$, $k_1 = 1$, $\alpha_2 = \varepsilon^{1/2}$, and $k_2 = \varepsilon^{3/2}$. Note that J in Eq. (19) has a negative sign in its expression shown in the Nomenclature section. This negative sign indicates species flux into the separator during discharge, when the electrode considered is the cathode.

Solution Procedure

In order to solve Eqs. (17)–(24), the Green's function associated with this problem must be determined first. The general form of the Green's function for multi-layer geometries can be written as follows [50]:

$$G_{ij}(x,t|x',t')_{t'=0} = \sum_{n=1}^{\infty}\frac{1}{N_n}\frac{k_j}{\alpha_j}\Gamma_n(t)\psi_{in}(x)\psi_{in}(x') \tag{25}$$

$$G_{ij}(x,t|x',t') = \sum_{n=1}^{\infty}\frac{1}{N_n}\frac{k_j}{\alpha_j}\Gamma_n(t-t')\psi_{in}(x)\psi_{in}(x') \tag{26}$$

where x'^p is the Sturm–Liouville weight function, and N_n is the norm, given by:

$$N_n = \sum_{j=1}^{M}\frac{k_j}{\alpha_j}\int_{x=x_j}^{x_{j+1}} x^p\psi_{jn}^2(x)dx \tag{27}$$

In order to construct the Green's function associated with this problem, $\Gamma(t)$ and $\psi(x)$ are determined by solving the corresponding homogeneous problem. Note that the term $J(t)$ in the governing equation, Eq. (18), and the boundary condition, Eq. (19) becomes zero in the corresponding homogeneous problem. The SOV technique can be used to solve the homogeneous problem; based on which, the concentration profile in the separator and electrode for the homogeneous problem can be written as follows:

$$c_{h,i}(x,t) = \sum_{n=0}^{\infty}\psi_{in}(x)\Gamma_n(t) \tag{28}$$

where $i = 1, 2$.

Equation (28) is then substituted back into the governing equations, which results in two separate differential equations in space and time. The solutions for time-dependent and space-dependent components of Eq. (28) can be written as:

$$\Gamma_n(t) = exp(-\lambda_n^2 t) \tag{29}$$

$$\psi_{1n}(x) = A_{1n}sin\left(\frac{\lambda_n x}{\sqrt{\alpha_1}}\right) + B_{1n}cos\left(\frac{\lambda_n x}{\sqrt{\alpha_1}}\right) \tag{30}$$

$$\psi_{2n}(x) = A_{2n}sin\left(\frac{\lambda_n x}{\sqrt{\alpha_2}}\right) + B_{2n}cos\left(\frac{\lambda_n x}{\sqrt{\alpha_2}}\right) \tag{31}$$

Note that α_1 and α_2 are already defined in the previous section. Using boundary conditions, a set of equations can be written in a matrix form for the unknown coefficients A_{in} and B_{in} as follows:

$$\begin{bmatrix} 1 & 0 & 0 & 0 \\ 0 & cos\frac{\lambda_n}{\sqrt{\alpha_1}} & -sin\frac{\lambda_n}{\sqrt{\alpha_2}} & -cos\frac{\lambda_n}{\sqrt{\alpha_2}} \\ 0 & Ksin\frac{\lambda_n}{\sqrt{\alpha_1}} & cos\frac{\lambda_n}{\sqrt{\alpha_2}} & -sin\frac{\lambda_n}{\sqrt{\alpha_2}} \\ 0 & 0 & cos\frac{\lambda_n(1+r)}{\sqrt{\alpha_2}} & -sin\frac{\lambda_n(1+r)}{\sqrt{\alpha_2}} \end{bmatrix} \begin{bmatrix} A_{1n} \\ B_{1n} \\ A_{2n} \\ B_{2n} \end{bmatrix} = \begin{bmatrix} 0 \\ 0 \\ 0 \\ 0 \end{bmatrix} \tag{32}$$

where $K = \frac{k_1}{k_2}\sqrt{\frac{\alpha_2}{\alpha_1}} = \varepsilon^{-5/4}$. In order to determine the eigenvalues, λ_n, the determinant of the matrix in Eq. (32) must be equal to zero, in order to result in a nontrivial solution. This requirement results in a transcendental equation for the eigenvalues as follows:

$$tan\left(\frac{\lambda_n r}{\sqrt{\alpha_2}}\right) + Ktan\left(\frac{\lambda_n}{\sqrt{\alpha_1}}\right) = 0 \tag{33}$$

Without loss of generality, any one of the non-vanishing coefficients in Eq. (44) may be set to unity. In this case, B_{1n} is chosen to be equal to 1. Consequently, the coefficients, A_{in} and B_{in}, are determined to be:

$$A_{1n} = 0 \tag{34}$$

$$B_{1n} = 1 \tag{35}$$

$$A_{2n} = cos\frac{\lambda_n}{\sqrt{\alpha_1}}sin\frac{\lambda_n}{\sqrt{\alpha_2}} - Ksin\frac{\lambda_n}{\sqrt{\alpha_1}}cos\frac{\lambda_n}{\sqrt{\alpha_2}} \tag{36}$$

$$B_{2n} = cos\frac{\lambda_n}{\sqrt{\alpha_1}}cos\frac{\lambda_n}{\sqrt{\alpha_2}} + Ksin\frac{\lambda_n}{\sqrt{\alpha_1}}sin\frac{\lambda_n}{\sqrt{\alpha_2}} \tag{37}$$

This completes the derivation of the solution. Using Eqs. (25) and (26), the concentration profile in the separator and electrode layers can be written as:

$$\begin{aligned} c_1(x,t) = \sum_{n=0}^{\infty} \Bigg(& \int_{x'=0}^{x'=1} \frac{1}{N_n}\exp\left(-\lambda_n^2 t\right)\cos\left(\frac{\lambda_n x}{\sqrt{\alpha_1}}\right)\cos\left(\frac{\lambda_n x'}{\sqrt{\alpha_1}}\right) f_1(x')dx' + \int_{x'=1}^{x'=1+r} \frac{1}{N_n}\exp\left(-\lambda_n^2 t\right)\cos\left(\frac{\lambda_n x}{\sqrt{\alpha_1}}\right)\left(A_{2n}\sin\left(\frac{\lambda_n x'}{\sqrt{\alpha_2}}\right)\right. \\ & \left. + B_{2n}\cos\left(\frac{\lambda_n x'}{\sqrt{\alpha_2}}\right)\right) f_2(x')dx' + \frac{\alpha_2}{k_2}\int_{\tau=0}^{\tau}\int_{x'=1}^{1+r} \frac{1}{N_n}\exp\left(-\lambda_n^2(t-t')\right)\cos\left(\frac{\lambda_n x}{\sqrt{\alpha_1}}\right)\left(A_{2n}\sin\left(\frac{\lambda_n x'}{\sqrt{\alpha_2}}\right)\right. \\ & \left. + B_{2n}cos\left(\frac{\lambda_n x'}{\sqrt{\alpha_2}}\right)\right) J(t')x'pdx'd\tau' + \frac{\alpha_2}{k_2}\int_{t'=0}^{t'=t} \frac{1}{N_n}\exp\left(-\lambda_n^2(t-t')\right)\cos\left(\frac{\lambda_n x}{\sqrt{\alpha_1}}\right)\left(A_{2n}\sin\left(\frac{\lambda_n(1+r)}{\sqrt{\alpha_2}}\right)\right) \\ & \left. + B_{2n}\cos\left(\frac{\lambda_n(1+r)}{\sqrt{\alpha_2}}\right)\right)(-rJ(t'))dt'\Bigg) \end{aligned} \tag{38}$$

$$\begin{aligned} c_2(x,t) = \sum_{n=0}^{\infty} & \int_{x'=0}^{x'=1} \frac{1}{N_n}\exp\left(-\lambda_n^2 t\right)\left(A_{2n}\sin\left(\frac{\lambda_n x}{\sqrt{\alpha_2}}\right) + B_{2n}\cos\left(\frac{\lambda_n x}{\sqrt{\alpha_2}}\right)\right)\cos\left(\frac{\lambda_n x'}{\sqrt{\alpha_1}}\right) f_1(x')dx' \\ & + \int_{x'=1}^{x'=1=r} \frac{1}{N_n}\exp\left(-\lambda_n^2 t\right)\left(A_{2n}\sin\left(\frac{\lambda_n x}{\sqrt{\alpha_2}}\right) + B_{2n}\cos\left(\frac{\lambda_n x}{\sqrt{\alpha_2}}\right)\right)\left(A_{2n}\sin\left(\frac{\lambda_n x'}{\sqrt{\alpha_2}}\right)\right. \\ & \left. + B_{2n}\cos\left(\frac{\lambda_n x'}{\sqrt{\alpha_2}}\right)\right) F_2(x')dx' + \frac{\alpha_2}{k_2}\int_{\tau=0}^{\tau}\int_{x'=1}^{1+r} \frac{1}{N_n}\exp\left(-\lambda_n^2(t-t')\right)\left(A_{2n}\sin\left(\frac{\lambda_n x}{\sqrt{\alpha_2}}\right)\right. \\ & \left. + B_{2n}\cos\left(\frac{\lambda_n x}{\sqrt{\alpha_2}}\right)\right)\left(A_{2n}\sin\left(\frac{\lambda_n x'}{\sqrt{\alpha_2}}\right) + B_{2n}\cos\left(\frac{\lambda_n x'}{\sqrt{\alpha_2}}\right)\right) J(t')x'pdx'd\tau' \\ & + \frac{\alpha_2}{k_2}\int_{t'=0}^{t'=t} \frac{1}{N_n}\exp\left(-\lambda_n^2(t-t')\right)\left(A_{2n}\sin\left(\frac{\lambda_n x}{\sqrt{\alpha_2}}\right)\right. \\ & \left. + B_{2n}\cos\left(\frac{\lambda_n x}{\sqrt{\alpha_2}}\right)\right)\left(A_{2n}\sin\left(\frac{\lambda_n(1+r)}{\sqrt{\alpha_2}}\right) + B_{2n}\cos\left(\frac{\lambda_n(1+r)}{\sqrt{\alpha_2}}\right)\right)(-rJ(t')dt') \end{aligned} \tag{39}$$

where A_{2n} and B_{2n} are defined in Eqs. (36) and (37), and N_n is defined in Eq. (27). Note that the zeroth terms of Eqs. (38) and (39), as well as the norm for the zeroth term, must be determined by calculating the limits of these equations as $\lambda \to 0$. Furthermore, note that if initial concentrations f_1 and f_2 are zero, there is some simplification in Eqs. (38) and (39).

Next, the validation of the model and its applications in a variety of realistic scenarios will be discussed. All plots in the next section are generated for a cathode.

Results and Discussion

Model Validation

Analytical model derived in the previous section is validated against past work and numerical simulations. To the best of our knowledge, no literature is available for solution-phase diffusion under time-dependent flux boundary condition. Therefore, comparison with past studies has been carried out for a special case of galvanostatic boundary condition where the applied current density is constant.

Green's function-based model presented in this study is compared against a past work by Subramanian et al. [51], where an approximate method was used to solve the solution-phase diffusion in the porous electrode [51]. Note that their method was limited to galvanostatic boundary conditions where the current density is constant. Thus, comparison of the present model against this previous study is carried out for a special case of constant current density. For comparison, a composite electrode comprising a porous cathode, separator, and Li-ion foil similar to Fig. 1 operating under a galvanostatic discharge boundary condition is considered. The parameters used for comparison are listed in Table 1, consistent with Subramanian et al. [51]. Figure 3(a) plots the non-dimensional concentration as a function of non-dimensional time at the electrode/separator interface, $x = 1$, for multiple values of current density for both the present model and previous work [51]. Figure 3(b) presents a similar plot at the current collector, $x = 1 + r$ for both models. Results show excellent agreement between the Green's function solution and past work. These figures show, as expected, that concentration at the separator-electrode interface increases with time, while concentration at the end of the electrode decreases with time. This is consistent with species consumption occurring throughout the electrode and species flux into the electrode only from the separator side. The rate of change of concentration increases with increasing current, and a steady-state concentration is reached in each case. As expected, the larger the current, the greater/lower is the concentration at $x = 1$ and $x = 1 + r$, respectively.

Table 1 Electrochemical and physical properties used in this study

Properties	Values	Units
D	2.6×10^{-10}	$m^2\ s^{-1}$
F	96,487	$C\ mol^{-1}$
t^+	0.2	-
ε	0.35	-
L_s	25×10^{-6}	m
L_c	125×10^{-6}	m
C_0	1000	$mol\ m^{-3}$
r	5	-

To further validate the analytical model presented here, a numerical simulation of solution-phase diffusion limitation in the composite porous electrode is carried out. The numerical method solves Eqs. (17)–(24) using a fully implicit approach to discretize the governing equations and boundary conditions in both separator and porous electrode, resulting in m number of equations where m is the number of nodes. Each equation contains three unknowns including the concentration of the *ith* point and its two neighbors for the next time, $n + 1$. Initial and boundary conditions, on the other hand, provide the known values for these equations. Spatial discretization is carried out in a way that ensures that a node is always present at the intersection between layers. Interface conditions are defined to ensure the continuity of concentration and flux at the separator/electrode interface. The resultant equations in the matrix form are solved using tri-diagonal matrix (TDMA) algorithm instead of direct inversion to reduce the computational time. A total of 2000 nodes are found to sufficiently ensure mesh independence of computed results. Figure 4(a) compares the non-dimensional concentration as a function of non-dimensional time at the current collector, $x = 1 + r$, determined from the Green's function approach with numerical simulations. This comparison is carried out for multiple values of B for a linear time-dependent current density, $I(t) = I_0(1 + B \cdot t)$ where $I_0 = 60\ Am^{-2}$. The plot shows very good agreement between the Green's function-based model and numerical solution for each case. Figure 4(a) shows that as the current density increases over time due to the slope B, the concentration at the back of the electrode, $x = 1 + r$, decreases faster, which consistent with results from Subramanian et al. [51]. The rate of reduction in concentration is greater for higher values of B, as expected. Figure 4(b) plots the non-dimensional concentration as a function of non-dimensional distance, x, at multiple times for the same current density profile as Fig. 4(a) and $B = 1/30$. Similar to Fig. 4(a), results show good agreement between the present analytical model and numerical simulations. The concentration behavior agrees well with results presented in a study by Subramanian and White [31], in which, an exact solution for solution-phase diffusion in composite electrodes under galvanostatic boundary conditions was derived. Results from the present work and [31] both show that as time passes, concentration increases in the separator due to the incoming flux from negative electrode, while the concentration deceases at the back of the electrode due to consumption of Li-ions.

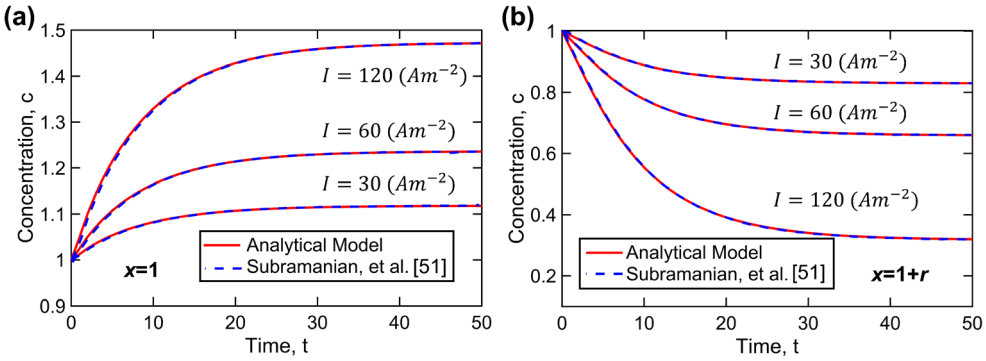

Fig. 3 Validation against previous study [51] for a special case of constant current density. **a** Dimensionless concentration at the electrode/separator interface ($x = 1$) as a function of dimensionless time for different rates of discharge. **b** Dimensionless concentration at the current collector ($x = 1 + r$) as a function of dimensionless time for different rates of discharge

Application of the Model

In this section, the Green's function solution is used to address a number of practical problems in which time-dependent boundary conditions may occur. Among different possible types of time-dependent functions, sinusoidal and step functions may be particularly relevant to battery operation. Sinusoidal functions are important since a reasonably well-behaved time-varying function may be expressed in the form of a Fourier series comprising sinusoidal functions. Another important type of boundary conditions relevant to operation of Li-ion cells is step functions, since sudden changes in charge/discharge rate may be encountered in realistic settings. Therefore, this section focuses specifically on problems with sinusoidal and step function boundary conditions.

First, discharge process for a porous cathode is considered, with a time-dependent sinusoidal current density, $I(t) = I_0(1 + \sin(2\pi\omega t)$ where $I_0 = 60\ \mathrm{Am}^{-2}$. Two different frequencies $\omega = 1/60$ & $\omega = 1/30$ are considered. All other problem parameters are similar to previous figures and summarized in Table 1. Figure 5(a) plots non-dimensional concentration as a function of time at three different locations—$x = 0$, 1, and $1 + r$—for the two frequencies. Results show a periodic behavior for concentration consistent with the sinusoidal current density. Figure 5(b) presents a plot of non-dimensional concentration as a function of non-dimensional distance at multiple times for $I_0 = 60\ \mathrm{Am}^{-2}$ and $\omega = 1/30$. Figure 5(b) shows an interesting behavior with intersections at multiple points. The concentration in the separator region is maximum at $t = 40$, minimum at $t = 60$, and in between at $t = 20$. This behavior reverses in the region close to the back of the electrode, $x = 1 + r$. This can be explained with the help of Fig. 5(a). For instance, in Fig. 5(a), at $t = 60$, due to the periodic nature of the current density, the concentration at the back of the electrode is close to its maximum whereas the concentration at $x = 0$ and 1 are close to their respective minima. These figures show that the model is successfully able to capture the concertation profiles under a sinusoidal time-dependent current density.

In order to more comprehensively capture the concentation profile throughout the composite electrode at different times, Fig. 6 shows a colorplot of concentration as a function of time and space, with the same current density profile as Fig. 5, and $\omega = 1/15$. It is seen that four maxima/minima occur up to $t = 60$, which is consistent with the frequency of the sinusoidal current density.

Figures 7 and 8 present plots for applications where the current density profile can be represented by step functions. This scenario may occur, for example, in the battery pack of an electric vehicle, where the discharge rate may suddenly change due to changes in the external load. Furthermore, in

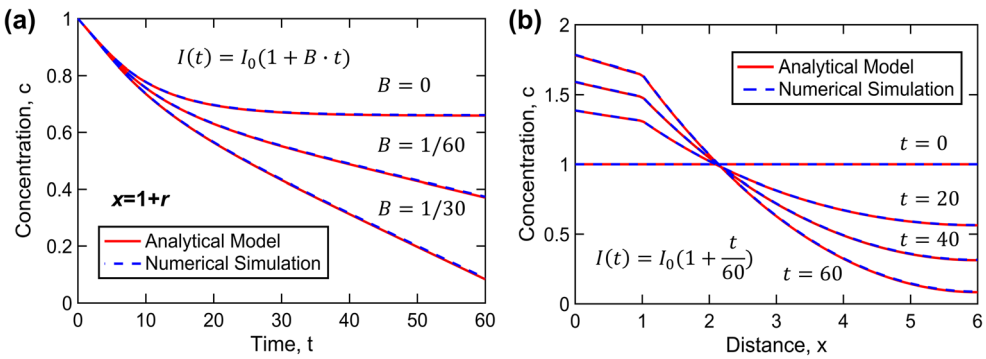

Fig. 4 Validation against numerical simulation for a linear current density $I(t) = I_0(1 + B \cdot t)$ where $I_0 = 60\ \mathrm{Am}^{-2}$. **a** Dimensionless concentration at the current collector ($x = 1 + r$) as a function of dimensionless time for different values of slopes, B. **b** Dimensionless concentration as a function of dimensionless distance at multiple times for $B = 1/60$

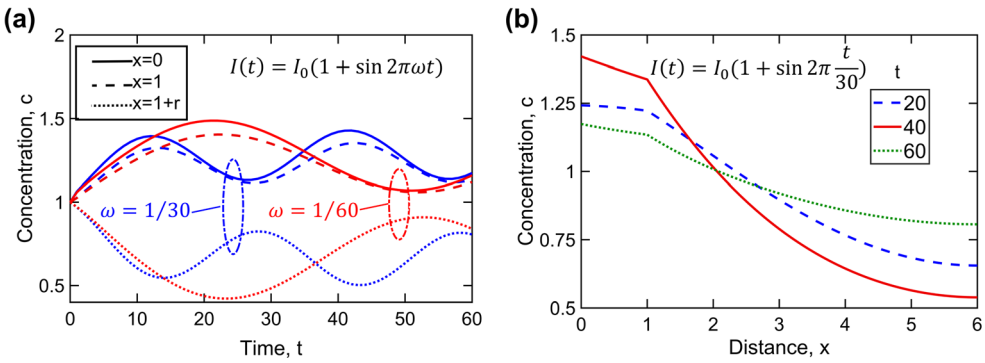

Fig. 5 Application of the model for a periodic current density $I(t) = I_0(1 + \sin 2\pi\omega t)$ where $I_0 = 60$ Am^{-2}. **a** Dimensionless concentration at multiple location as a function of dimensionless time for $\omega = 1/30$ and 1/60. **b** Dimensionless concentration as a function of dimensionless distance at multiple times for $\omega = 1/30$

several commonly used charge/discharge protocols, Li cells may be cyclically charged and discharged at different rates, so that the current density may change its magnitude and/or direction over time. Two specific cases are presented in Figs. 7 and 8.

Figure 7 presents concentration plots for a step-function boundary condition, with changes only in the magnitude of current, and not the direction. In this case, the current density function is a three-step discharge process at multiple discharge rate of 60, 120, and 180 Am^{-2} corresponding to C-rates of 1, 2, and 3, respectively. Figure 7(a) plots non-dimensional concentration as a function of non-dimensional time at three different locations, whereas Fig. 7(b) presents the plot of non-dimensional concentration as a function of non-dimensional distance at multiple times. It is seen from Fig. 7(a) that the concentration at the back of the electrode decreases gradually and the rate of this reduction increases with increasing magnitude of current density. On the other hand, concentration in the separator increases with time. This is due to concentration flux into the separator during the discharge process, and simultaneous depletion of species in the electrode due to reaction. As expected from the current density profile, Fig. 7(b) shows that concentration at the back of the electrode is lowest at the highest discharge rate and the concentration in the separator is highest at the highest discharge rate.

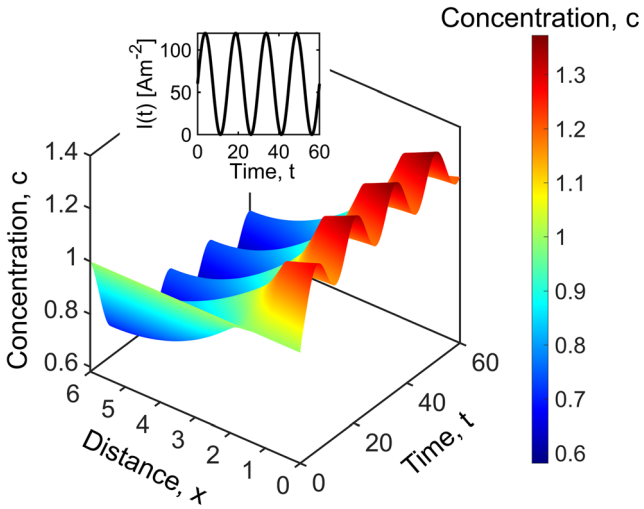

Fig. 6 Application of the model for a periodic current density $I(t) = I_0(1 + \sin 2\pi\omega t)$ where $I_0 = 60$ Am^{-2} and $\omega = 1/15$. Three dimensional plot of concentration as functions of space and time

Figure 8 considers a somewhat more complicated scenario, in which the current density starts with a constant discharge at 60 Am^{-2}, switches directions to a 40-Am^{-2} charge at $t = 20$, and finally changes back to 120 Am^{-2} discharge at $t = 40$. Figure 8(a) plots the computed non-dimensional concentration for this case as a function of non-dimensional time at three different locations, $x = 0$, 1, and $1 + r$. For reference, the current density profile as a function of time is also plotted in the inset. It is seen that concentration at the back of the electrode decreases in the beginning for $t < 20$ (discharge), and increases as the current density switches directions in the $20 < t < 40$ period (charge). Finally, the concentration at $x = 1 + r$ decreases again for $t > 40$ (discharge), consistent with the current density profile. Concentration profiles at the other two locations, $x = 0$ and $x = 1$, exhibit the opposite trend, which is consistent with concentration flux dominating over species consumption due to intercalation in the electrode. Figure 8(b) presents a plot of dimensionless concentration throughout the composite electrode at multiple times. Concentration profiles are plotted at $t = 20$, 40, and 60. Results in this plot are consistent with Fig. 8(a). The maximum concentration in the electrode occurs at $t = 40$, consistent with the inset plot of current density.

Note that all results presented here are computed with only five eigenvalues. This helps significantly reduce the computational time, particularly when the operating condition is a complicated function of time. The use of more than five eigenvalues is found to result in no significant change in the computed concentration distribution. It is important to note that eigenvalues for this problem

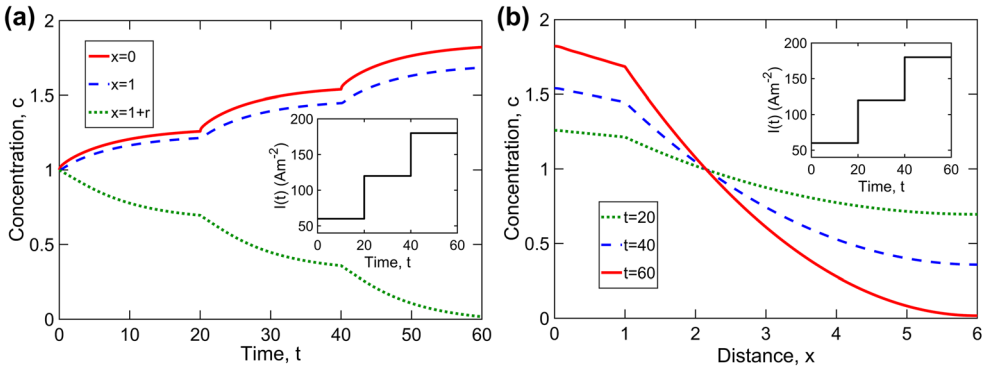

Fig. 7 Application of the model for a step function discharge current density. **a** Dimensionless concentration as a function of dimensionless time at multiple locations, $x = 0$, 1, and $1 + r$. **b** Dimensionless concentration as a function of dimensionless distance at multiple times, $t = 20$, 40, and 60

depend only on r and ε, and therefore, once the values of these parameters are known, the eigenvalues can be calculated once and be used for any arbitrary boundary condition. Table 2 presents the first five eigenvalues for $\varepsilon = 0.35$ and multiple values of r.

Conclusions

In this paper, the Green's function approach is used to derive an analytical solution for solution-phase limitation diffusion in composite electrodes under a wide variety of time-dependent flux boundary conditions. The method is applied to a composite electrode consisting of Li-ion foil, separator, and porous electrode similar to the composite Li-ion cell sandwich proposed by Doyle and Newman [22]. Concentration profiles in the separator and porous electrode are determined as functions of space and time. The mathematical model is validated against previous studies for the special case of galvanostatic boundary conditions. Furthermore, Green's function-based model is validated by comparison with numerical simulations for time-dependent boundary conditions. The mathematical model presented in this study can be used to accurately predict the transient behavior of solution-phase limitation diffusion. The model is used to predict the concentration profile for a number of realistic time-dependent current densities such as sinusoidal and step functions that may be encountered in practical energy conversion and storage. The computational time associated with the present model is lower than numerical simulations due to the low number of eigenvalues required for convergence. This work contributes towards the theoretical understanding of species diffusion in Li-ion cells, and provides tools that may be helpful for designing, predicting, and improving the performance of electrochemical devices.

Acknowledgments The authors would like to gratefully acknowledge useful discussions with Prof. Venkat Subramanian, Dr. Manan Pathak, and Qiu Teo.

Authors' Contributions Mohammad Parhizi – methodology, formal analysis, investigation, data curation, visualization; Ankur Jain – conceptualization, methodology, supervision, project administration, visualization, funding acquisition; All authors contributed towards writing the original draft and review/editing.

Funding This material is based upon work supported by CAREER Award No. CBET-1554183 from the National Science Foundation.

Availability of Data and Material Data and material are available upon request from the corresponding author.

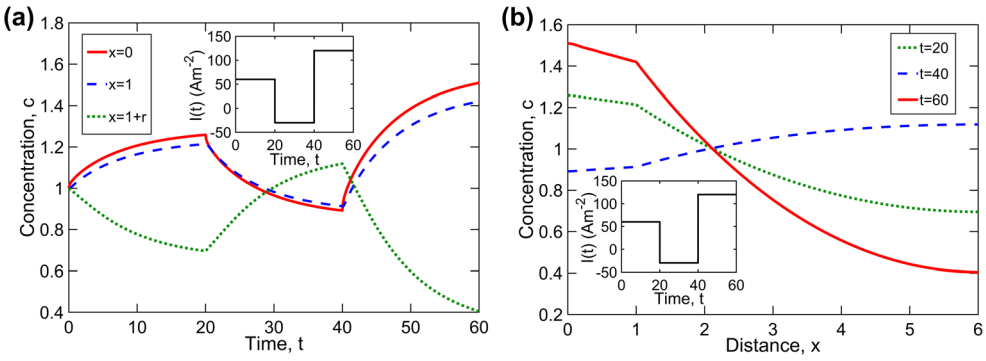

Fig. 8 Application of the model for a cyclic step function current density. **a** Dimensionless concentration as a function of dimensionless time at multiple locations, $x = 0$, 1, and $1 + r$. **b** Dimensionless concentration as a function of dimensionless distance at multiple times, $t = 20$, 40, and 60

Table 2 Values of eigenvalues for $\varepsilon = 0.35$ for multiple values of r

r	λ_1	λ_2	λ_3	λ_4	λ_5
4	0	0.408935	0.943229	1.513226	2.085300
5	0	0.341385	0.766828	1.223153	1.686654
6	0	0.294434	0.647903	1.02749	1.414978
8	0	0.232656	0.497336	0.780636	1.071196
10	0	0.193285	0.405536	0.631237	0.863146

Compliance with Ethical Standards

Conflict of Interest None.

Code Availability Not applicable.

References

1. Goodenough JB, Park K-S (2013) ChemInform abstract: the li-ion rechargeable battery: a perspective. ChemInform 44. https://doi.org/10.1002/chin.201320273
2. Scrosati B, Garche J (2010) Lithium batteries: status, prospects and future. J Power Sources 195:2419–2430. https://doi.org/10.1016/j.jpowsour.2009.11.048
3. Dunn B, Kamath H, Tarascon J-M (2011) Electrical energy storage for the grid: a battery of choices. Science. 334:928–935. https://doi.org/10.1126/science.1212741
4. Pasquier AD, Plitz I, Menocal S, Amatucci G (2003) A comparative study of Li-ion battery, supercapacitor and nonaqueous asymmetric hybrid devices for automotive applications. J Power Sources 115:171–178. https://doi.org/10.1016/s0378-7753(02)00718-8
5. Johnson BA, White RE (1998) Characterization of commercially available lithium-ion batteries. J Power Sources 70:48–54. https://doi.org/10.1016/s0378-7753(97)02659-1
6. Parhizi M, Ahmed M, Jain A (2017) Determination of the core temperature of a Li-ion cell during thermal runaway. J Power Sources 370:27–35. https://doi.org/10.1016/j.jpowsour.2017.09.086
7. Shah K, Balsara N, Banerjee S, Chintapalli M, Cocco AP, Chiu WKS et al (2017) State of the art and future research needs for multiscale analysis of li-ion cells. J Electrochem Energy Convers Stor 14. https://doi.org/10.1115/1.4036456
8. Diouf B, Pode R (2015) Potential of lithium-ion batteries in renewable energy. Renew Energy 76:375–380. https://doi.org/10.1016/j.renene.2014.11.058
9. Zhang J, Lee J (2011) A review on prognostics and health monitoring of Li-ion battery. J Power Sources 196:6007–6014. https://doi.org/10.1016/j.jpowsour.2011.03.101
10. Sushko ML, Rosso KM, Zhang J-GJ, Liu J (2011) Multiscale simulations of Li ion conductivity in solid electrolyte. J Phys Chem Lett 2:2352–2356. https://doi.org/10.1021/jz201032w
11. Jokar A, Rajabloo B, Désilets M, Lacroix M (2016) Review of simplified pseudo-two-dimensional models of lithium-ion batteries. J Power Sources 327:44–55. https://doi.org/10.1016/j.jpowsour.2016.07.036
12. Xiong R, Cao J, Yu Q, He H, Sun F (2018) Critical review on the battery state of charge estimation methods for electric vehicles. IEEE Access 6:1832–1843. https://doi.org/10.1109/access.2017.2780258
13. Botte GG, Subramanian VR, White RE (2000) Mathematical modeling of secondary lithium batteries. Electrochim Acta 45:2595–2609. https://doi.org/10.1016/s0013-4686(00)00340-6
14. Doyle M (1993) Modeling of galvanostatic charge and discharge of the lithium/polymer/insertion cell. J Electrochem Soc 140:1526–1533. https://doi.org/10.1149/1.2221597
15. Newman J, Thomas-Alyea KE (2012) Electrochemical systems. Wiley
16. Fuller TF, Newman JA (1989) Concentrated solution theory model of transport in solid–polymer–electrolyte fuel cells. Electrochem Soc Proc Ser 89–14
17. Ramadesigan V, Northrop PWC, De S, Santhanagopalan S, Braatz RD, Subramanian VR (2012) Modeling and simulation of lithium-ion batteries from a systems engineering perspective. J Electrochem Soc 159. https://doi.org/10.1149/2.018203jes
18. Ning G, Popov BN (2004) Cycle life modeling of lithium-ion batteries. J Electrochem Soc 151. https://doi.org/10.1149/1.1787631
19. Santhanagopalan S, Guo Q, Ramadass P, White RE (2006) Review of models for predicting the cycling performance of lithium ion batteries. J Power Sources 156:620–628. https://doi.org/10.1016/j.jpowsour.2005.05.070
20. Ramadesigan V, Boovaragavan V, Subramanian VR (2009) Efficient reformulation of solid-phase diffusion in physics-based lithium-ion battery models. ECS Trans. https://doi.org/10.1149/1.3115314
21. Rahimian SK, Rayman S, White RE (2013) Extension of physics-based single particle model for higher charge–discharge rates. J Power Sources 224:180–194. https://doi.org/10.1016/j.jpowsour.2012.09.084
22. Doyle M, Newman J (1997) Analysis of capacity–rate data for lithium batteries using simplified models of the discharge process. J Appl Electrochem 27:846–856. https://doi.org/10.1023/A:1018481030499
23. Smith KA, Rahn CD, Wang C-Y (2008) Model order reduction of 1D diffusion systems via residue grouping. J Dyn Syst Meas Control 130. https://doi.org/10.1115/1.2807068
24. Subramanian VR, Ritter JA, White RE (2001) Approximate solutions for galvanostatic discharge of spherical particles I. Constant diffusion coefficient. J Electrochem Soc 148. https://doi.org/10.1149/1.1409397
25. Domenico DD, Fiengo G, Stefanopoulou A (2008) Lithium-ion battery state of charge estimation with a Kalman Filter based on a electrochemical model, 2008 IEEE International Conference on Control Applications. https://doi.org/10.1109/cca.2008.4629639
26. Smith KA, Rahn CD, Wang C-Y (2007) Control oriented 1D electrochemical model of lithium ion battery. Energy Convers Manag 48:2565–2578. https://doi.org/10.1016/j.enconman.2007.03.015
27. Luo W, Lyu C, Wang L, Zhang L (2013) A new extension of physics-based single particle model for higher charge–discharge rates. J Power Sources 241:295–310. https://doi.org/10.1016/j.jpowsour.2013.04.129
28. Guo M, White RE (2012) An approximate solution for solid-phase diffusion in a spherical particle in physics-based Li-ion cell models. J Power Sources 198:322–328. https://doi.org/10.1016/j.jpowsour.2011.08.096
29. Luo W, Lyu C, Wang L, Zhang L (2013) An approximate solution for electrolyte concentration distribution in physics-based lithium-ion cell models. Microelectron Reliab 53:797–804. https://doi.org/10.1016/j.microrel.2012.11.002
30. Cai L, White RE (2009) Reduction of model order based on proper orthogonal decomposition for lithium-ion battery simulations. J Electrochem Soc 156. https://doi.org/10.1149/1.3049347
31. Subramanian VR, White RE (2001) New separation of variables method for composite electrodes with galvanostatic boundary conditions. J Power Sources 96:385–395. https://doi.org/10.1016/s0378-7753(00)00656-x

32. Liu S (2006) An analytical solution to Li/Li insertion into a porous electrode. Solid State Ionics 177:53–58. https://doi.org/10.1016/j.ssi.2005.09.053
33. Johan MR, Arof AK (2004) Analytical solution to the material balance equation by integral transform for different cathode geometries. Ionics. 10:405–414. https://doi.org/10.1007/bf02378001
34. Ali SH, Hussin A, Arof A (2002) Short- and long-time solutions for material balance equation in lithium-ion batteries by Laplace transform. J Power Sources 112:435–442. https://doi.org/10.1016/s0378-7753(02)00420-2
35. Johan MR, Arof AK (2007) Modeling of electrochemical intercalation of lithium into a LiMn2O4 electrode using Green function. J Power Sources 170:490–494. https://doi.org/10.1016/j.jpowsour.2007.03.069
36. Johnston P (1991) Diffusion in composite media: solution with simple eigenvalues and eigenfunctions. Math Comput Model 15:115–123. https://doi.org/10.1016/0895-7177(91)90096-P
37. Hickson RI, Barry SI, Mercer GN (2009) Critical times in multilayer diffusion. Part 1: exact solutions. Int J Heat Mass Transf 52:5776–5783. https://doi.org/10.1016/j.ijheatmasstransfer.2009.08.013
38. Carr EJ, Turner IW (2016) A semi-analytical solution for multilayer diffusion in a composite medium consisting of a large number of layers. Appl Math Model 40:7034–7050
39. Mulholland GP, Cobble MH (1972) Diffusion through composite media. Int J Heat Mass Transf 15:147–160. https://doi.org/10.1016/0017-9310(72)90172-X
40. Pérez Guerrero JS, Pontedeiro EM, van Genuchten MT, Skaggs TH (2013) Analytical solutions of the one-dimensional advection–dispersion solute transport equation subject to time-dependent boundary conditions. Chem Eng J 221:487–491. https://doi.org/10.1016/j.cej.2013.01.095
41. Rodrigo MR, Worthy AL (2016) Solution of multilayer diffusion problems via the Laplace transform. J Math Anal Appl 444:475–502
42. Lin J, Chen CS, Liu C-S, Lu J (2016) Fast simulation of multi-dimensional wave problems by the sparse scheme of the method of fundamental solutions. Comput Math Appl 72:555–567
43. Lin J, Zhang C, Sun L, Lu J (2018) Simulation of seismic wave scattering by embedded cavities in an elastic half-plane using the novel singular boundary method. Adv Appl Math Mech 10:322–342
44. Choobineh L, Jain A (2015) An explicit analytical model for rapid computation of temperature field in a three-dimensional integrated circuit (3D IC). Int J Therm Sci 87:103–109. https://doi.org/10.1016/j.ijthermalsci.2014.08.012
45. Carr EJ, March NG (2018) Semi-analytical solution of multilayer diffusion problems with time-varying boundary conditions and general interface conditions. Appl Math Comput 333:286–303
46. Parhizi M, Jain A (2020) Analytical modeling of solid phase diffusion in single-layer and composite electrodes under time-dependent flux boundary condition. J Electrochem Soc 167:060528. https://doi.org/10.1149/1945-7111/ab847c
47. Hahn DW, Özişik MN (2012) Heat conduction. Wiley, New York). https://doi.org/10.1002/9781118411285
48. Yang S, Meng Z, Peng G, Gong Y (2006) The solutions of Green's function of diffusion equation for three-layered matched medium in the steady state, Proc. 4th Int. Conf. Photonics & Imaging in Biology and Medicine 604706. https://doi.org/10.1117/12.709787
49. Kulkarni KN, Ram-Mohan LR, Dayananda MA (2007) Matrix Green's function analysis of multicomponent diffusion in multilayered assemblies. J Appl Phys 102:064908. https://doi.org/10.1063/1.2779235
50. K. Cole, J. Beck, A. Haji-Sheikh, B. Litkouhi, Heat conduction using Greens functions, (2010). https://doi.org/10.1117/12.709787
51. Subramanian VR, Tapriyal D, White RE (2004) A boundary condition for porous electrodes. Electrochem Solid-State Lett 7. https://doi.org/10.1149/1.1773751